Int. J. Heat Mass Transfer. Vol. 11, pp. 387–396. Pergamon Press 1968. Printed in Great Britain

NATURAL CONVECTION BETWEEN CONCENTRIC SPHERES AT LOW RAYLEIGH NUMBERS

LAWRENCE R. MACK and HARRY C. HARDEE†

The University of Texas, Austin, Texas, U.S.A.

(*Received* 20 *November* 1966 *and in revised form* 7 *August* 1967)

Abstract—With neglect of viscous heating and with treatment of each fluid property except specific weight as constant, the solution for steady axisymmetric natural convection between isothermal concentric spheres is obtained. Streamline configuration, velocity and temperature distributions, and both local and overall heat-transfer rates are discussed and illustrated. Appropriate comparisons are made with experimental results. Theory and experiment supplement one another; a design example is given in which both types of results are needed.

NOMENCLATURE

All primed quantities are dimensional; all unprimed quantities are dimensionless. Parenthetical presuperscripts indicate the scripted-order approximation to the quantity; see equations (26) and (27).

A, Rayleigh number, $g'\beta'(T_i' - T_o')R_i'^3/(\nu'\alpha')$;

A^*, Rayleigh number based on gap thickness, $g'\beta'(T_i' - T_o')(R_o' - R_i')^3/(\nu'\alpha')$;

A_{lim}, A^*_{lim}, limiting Rayleigh number; see Section 3.1;

g', acceleration of gravity;

k', thermal conductivity;

$\bar{N}$, overall Nusselt number, $Q'(R_o - 1)[4\pi k'(T_i' - T_o')R_i'R_o]^{-1}$;

$\bar{N}^*$, $= R_o(R_o - 1)^{-1}\bar{N}$; $R_i'k'^{-1}$ times an overall heat-transfer coefficient defined using the inner-sphere area;

N_i, inner-sphere local Nusselt number, $q_i'R_i'(R_o - 1)[k'R_o(T_i' - T_o')]^{-1}$;

N_o, outer-sphere local Nusselt number, $q_o'R_i'(R_o^2 - R_o)[k'(T_i' - T_o')]^{-1}$;

P, Prandtl number, ν'/α';

Q', overall heat-flow rate from inner to outer sphere, energy/time;

q_i', q_o', local radial heat-flow rates per unit area at inner and outer spheres, respectively, energy/(time–area);

R', R, radial coordinate, $R = R'/R_i'$;

R_i', R_o', radii of inner and outer spheres, respectively;

R_o, radius ratio, R_o'/R_i';

T', T, temperature, $T = (T' - T_o')/(T_i' - T_o')$;

T_i', T_o', temperatures of inner and outer spheres, respectively;

T_j, jth-order term in expansion of T, see equation (8);

V_R', V_R, R-component of velocity, $V_R = V_R'R_i'/\alpha'$;

V_θ', V_θ, θ-component of velocity, $V_\theta = V_\theta'R_i'/\alpha'$.

Greek symbols

α', thermal diffusivity;

β', volumetric coefficient of thermal expansion;

θ, colatitude or polar angle, measured from the upward vertical $\theta = 0$;

† Now at Sandia Corporation, Albuquerque, New Mexico.

ν', kinematic viscosity;
ψ', ψ, Stokes stream function, $\psi = \psi'/(\alpha' R_i')$;
ψ_j, jth-order term in expansion of ψ, see equation (9).

1. INTRODUCTION

SCANLAN and his colleagues experimentally investigated the natural convection of air enclosed between two concentric spheres, each of which was maintained at a different steady uniform temperature. Using techniques which they developed [1], Bishop, Kolflat, Mack and Scanlan [2] described flow patterns observed visually and recorded photographically. Temperature distributions, heat-transfer data, and additional comments on the flow patterns were presented by Bishop, Mack and Scanlan [3].

To predict the physical behavior for conditions not covered by the experimental work, and to gain further insight into the nature of the convective flow phenomena, it is desirable to have a theoretical analysis of the problem. For a particular type of transient flow Sevruk [4] obtained the first temperature term and the first velocity term in series expansions in powers of the Rayleigh number, but his mathematical expressions were so unwieldy that he could draw no physical conclusions. To the authors' knowledge there is available in the literature no theory which is both pertinent and usable.

Although an unsteady flow ("falling-vortices" regime) was observed under certain conditions, the experimental work [2, 3] indicated that the flow is both steady and axisymmetric for sufficiently low temperature differences. Guided in our assumptions by the experimental results, we give in the present paper an analysis of natural convection in the enclosure between concentric spheres for small differences in their temperatures. The particular aspects of the solution which will be discussed include the range of reliability of the solution, the configuration of the streamlines, the velocity and temperature distributions, and both local and overall heat-transfer rates. Where appropriate, comparison is made with experimental results.

2. THE PROBLEM AND ITS SOLUTION

2.1. *Governing equations*

We consider steady laminar natural convection of a fluid enclosed between two concentric spheres. The temperature of each sphere is uniform, the inner sphere being the hotter. We use spherical coordinates and we assume that all quantities are independent of the longitude and that the velocity has no longitudinal component. All fluid properties are treated as constants except the specific weight, a property which appears only in the buoyancy term, but which term represents the driving mechanism for the flow.

In terms of dimensionless quantities, the governing equations are

$$\mathrm{D}^4\psi = -AR\sin\theta\left(\sin\theta\frac{\partial T}{\partial R}+\frac{\cos\theta}{R}\frac{\partial T}{\partial\theta}\right)+\frac{1}{P}\sin\theta\left(\frac{\partial\psi}{\partial\theta}\frac{\partial}{\partial R}-\frac{\partial\psi}{\partial R}\frac{\partial}{\partial\theta}\right)\left(\frac{\mathrm{D}^2\psi}{R^2\sin^2\theta}\right), \quad (1)$$

$$\nabla^2 T = \frac{1}{R^2\sin\theta}\left(\frac{\partial\psi}{\partial\theta}\frac{\partial}{\partial R}-\frac{\partial\psi}{\partial R}\frac{\partial}{\partial\theta}\right)T, \quad (2)$$

$$\psi = \frac{\partial\psi}{\partial R} = 0 \quad \text{at } R = 1, R_o, \quad (3)$$

$$\psi = \frac{\partial\psi}{\partial\theta} = 0 \quad \text{at } \theta = 0, \pi, \quad (4)$$

$$T = 1 \quad \text{at } R = 1, \quad (5)$$

$$T = 0 \quad \text{at } R = R_o, \quad (6)$$

$$\frac{\partial T}{\partial\theta} = 0 \quad \text{at } \theta = 0, \pi, \quad (7)$$

where the operators D^4, D^2 and ∇^2 are given by $\mathrm{D}^4 = \mathrm{D}^2(\mathrm{D}^2)$,

$$\mathrm{D}^2 = \frac{\partial^2}{\partial R^2}+\frac{1}{R^2}\frac{\partial^2}{\partial\theta^2}-\frac{\cot\theta}{R^2}\frac{\partial}{\partial\theta},$$

$$\nabla^2 = \frac{\partial^2}{\partial R^2}+\frac{2}{R}\frac{\partial}{\partial R}+\frac{1}{R^2}\frac{\partial^2}{\partial\theta^2}+\frac{\cot\theta}{R^2}\frac{\partial}{\partial\theta}.$$

The differential equations (1) and (2) are coupled and nonlinear. Equation (1) is the vorticity equation obtained by taking the curl of the Navier–Stokes equation in order to eliminate the pressure-gradient term, while (2) is the energy equation with neglect of viscous heating. Use of the stream function instead of the R- and θ-components of velocity identically satisfies the continuity equation. Conditions (3) assure that both normal and tangential components of velocity vanish at the surface of each sphere; conditions (4) assure that the velocity is finite at the axis of symmetry $\theta = 0, \pi$ and that the velocity component normal to this axis vanishes. The spheres are specified isothermal by conditions (5) and (6), while (7) is necessary for the divergence of the heat flux to be finite at the vertical axis (i.e. for the rate of conduction of thermal energy per unit volume to be finite there).

2.2. *Method of solution*

In the present geometry the fluid cannot be in equilibrium for any non-zero temperature difference, no matter how small. It is thus possible to expand the dependent variables T and ψ in power series of the Rayleigh number:

$$T = \sum_{j=0}^{\infty} A^j T_j(R, \theta), \tag{8}$$

$$\psi = \sum_{j=1}^{\infty} A^j \psi_j(R, \theta). \tag{9}$$

Substituting equations (8) and (9) into the governing equations and equating coefficients of like powers of A, we obtain an infinite set of uncoupled linear differential equations to be solved in sequence:

$$\nabla^2 T_j = \frac{1}{R^2 \sin\theta} \sum_{k=1}^{j} \left(\frac{\partial \psi_k}{\partial \theta} \frac{\partial}{\partial R} - \frac{\partial \psi_k}{\partial R} \frac{\partial}{\partial \theta} \right) T_{j-k}, \tag{10}$$

$$\mathrm{D}^4 \psi_j = -R \sin\theta \left(\sin\theta \frac{\partial T_{j-1}}{\partial R} + \frac{\cos\theta}{R} \frac{\partial T_{j-1}}{\partial \theta} \right) + \frac{1}{P} \sin\theta \sum_{k=1}^{j-1} \left(\frac{\partial \psi_k}{\partial \theta} \frac{\partial}{\partial R} - \frac{\partial \psi_k}{\partial R} \frac{\partial}{\partial \theta} \right) \left(\frac{\mathrm{D}^2 \psi_{j-k}}{R^2 \sin^2\theta} \right). \tag{11}$$

Boundary condition (5) becomes

$$T_0 = 1 \quad \text{at } R = 1; \qquad T_j = 0 \quad \text{at } R = 1, \quad j \geqslant 1, \tag{12}$$

while the other boundary conditions are just equations (3), (4), (6), and (7) with ψ, T replaced by ψ_j, T_j for all j.

2.3. *Solution*

The first equation to be solved is $\nabla^2 T_0 = 0$ subject to conditions (6), (7) and (12). The solution,

$$T_0 = -(R_o - 1)^{-1} + R_o (R_o - 1)^{-1} R^{-1}, \tag{13}$$

gives the well known temperature distribution for pure conduction.

Substitution of (13) into the right side of (11) for $j = 1$ gives an equation whose solution satisfying conditions (3) and (4) is the creeping-flow result

$$\psi_1 = -\frac{R_o}{8(R_o - 1)} (B_1 R^4 + R^3 + B_2 R^2 + B_3 R + B_4 R^{-1}) \sin^2\theta, \tag{14}$$

where

$$B_1 = (2R_o^7 - 6R_o^6 + 4R_o^5 + 4R_o^4 - 6R_o^3 + 2R_o^2)/\Delta, \tag{15}$$

$$B_2 = (2R_o^9 - 12R_o^7 + 10R_o^6 + 10R_o^5 - 12R_o^4 + 2R_o^2)/\Delta, \tag{16}$$

$$B_3 = (-3R_o^9 + 8R_o^8 - 5R_o^7 - 5R_o^5 + 8R_o^4 - 3R_o^3)/\Delta, \tag{17}$$

$$B_4 = (R_o^9 - 4R_o^8 + 6R_o^7 - 4R_o^6 + R_o^5)/\Delta, \tag{18}$$

$$\Delta = -4R_o^8 + 9R_o^7 - 10R_o^5 + 9R_o^3 - 4R_o^2. \tag{19}$$

In a similar manner it may be shown that

$$T_1 = f_1(R)\cos\theta, \tag{20}$$

$$\psi_2 = f_2(R)\sin^2\theta\cos\theta, \tag{21}$$

$$T_2 = f_3(R)(3\cos^2\theta - 1) + f_4(R), \tag{22}$$

$$\psi_3 = f_5(R)(5\sin^2\theta\cos^2\theta - \sin^2\theta) + f_6(R)\sin^2\theta, \tag{23}$$

$$T_3 = f_7(R)(5\cos^3\theta - 3\cos\theta) + f_8(R)\cos\theta. \tag{24}$$

Each function $f_k(R)$, $1 \leqslant k \leqslant 8$, is a sum of a number of terms, each of the form $R^m(\ln R)^n$. The coefficients of these terms depend on the parameter R_o and, in general, on P. However, we note that f_1 and f_4, like the expressions in equations (13) and (14), are independent of P. The expressions for the f_k are long and are omitted to conserve space; details may be found in the dissertation of Hardee [5].

3. DISCUSSION

For mathematical analysis it is convenient to use a Rayleigh number A based on the radius of the inner sphere. For experimental work, however, a Rayleigh number A^* based on the distance $R_o' - R_i'$ between the spheres and related to A by $A^* = (R_o - 1)^3 A$ is commonly used.

Although we considered the inner sphere to be the hotter surface in the formulation of the problem, the case for which the outer sphere is the hotter may be obtained from our solution merely by use of negative values of A.

3.1. *Range of reliability of the solution*

As a crude measure of the upper bound for convergence (as opposed to *useful* convergence) of the series expansions (8) and (9), we define A_{lim} as that value of Rayleigh number for which the maximum (with respect to position) magnitude of any higher-order term in either series equals the maximum magnitude of the appropriate lowest-order term, T_0 or $A\psi_1$. This value A_{lim} is a function of only R_o and P. Numerical investigation for five values of R_o indicated that, for any Prandtl number in the range $P \geqslant 0{\cdot}70$, A_{lim} decreases monotonically from about $2{\cdot}75 \times 10^6$ to about 275 as R_o increases from 1·15 to 3·00. (Throughout the numerical computations of this paper, double-precision methods were found necessary.) This variation may be expressed roughly by the approximate empirical relation

$$A_{\text{lim}} \approx 3 \times 10^{\{3\,-\,[\ln(R_o\,-\,1)]/\ln 2\}} \quad \text{for } 1{\cdot}15 \leqslant R_o \leqslant 3.00,\ P \geqslant 0{\cdot}70. \tag{25}$$

For $P = 0{\cdot}02$, A_{lim} is about $\frac{1}{20}$–$\frac{1}{10}$ of the value given by equation (25). If it is desired to consider the Rayleigh number based on gap thickness, it may be shown that (for $P \geqslant 0{\cdot}70$) A^*_{lim} decreases from about 9300 to about 2200 as R_o increases from 1·15 to 3·00.

The maximum usable Rayleigh number for the series of equations (8) and (9) to converge rapidly enough so as to represent accurately the true T and ψ when truncated after the terms for $j = 3$ was arbitrarily (and probably somewhat conservatively) considered to be approximately one-third of A_{lim}. We cannot prove convergence of the series expansions; however, with A_{lim} defined in the above manner, there is good indication that the series will converge and yield reliable results for $A \leqslant A_{\text{lim}}/3$.

To give better indication of the reliability of the solution, we outline an error analysis. Let ${}^{(m)}\psi$ and ${}^{(n)}T$ denote the mth approximation to ψ and the nth approximation to T, respectively, where

$${}^{(m)}\psi = \sum_{j=1}^{m} A^j\psi_j, \tag{26}$$

$${}^{(n)}T = \sum_{j=0}^{n} A^j T_j. \tag{27}$$

Since the finite approximations are in general not equal to the true ψ and T, the quantities ${}^{(m)}\psi$ and ${}^{(n)}T$, when substituted for ψ and T, will not satisfy the differential equations (1) and (2) for all R and θ. We define a positive-definite error measure F_{mn} for equation (1) as the volume integral over the fluid domain of the absolute

value of the difference between the two sides of equation (1) when ${}^{(m)}\psi$, ${}^{(n)}T$ are used for ψ, T; a positive-definite error measure G_{mn} for equation (2) is similarly defined. The error measures F_{mn} and G_{mn} are functions solely of the system parameters A, P and R_o. Convergence of the solution for $A \leqslant A_{\text{lim}}/3$ is strongly implied by the fact that the net result of increasing the order of approximation both to ψ and to T by one is a significant reduction in the magnitudes of both error measures. (Numerical illustration is given by Hardee [5].)

3.2. *Streamline configuration*

To the order in Rayleigh number through which the solution has been carried, the best approximation for the stream function is ${}^{(3)}\psi$ [see equation (26)]. The streamlines as given by ${}^{(3)}\psi$ for $A = 1000$, $P = 0{\cdot}70$ (approximately the value for air), and $R_o = 2{\cdot}00$ are presented in Fig. 1. (In order to provide a relatively complete description of the convective phenomena for a particular case, we shall use these same values of the parameters in illustrating other aspects of the solution in Sections 3.3, 3.4 and 3.5.) It is observed that Fig. 1 shows a single cell of the "crescent-eddy" type which was photographed and described by Bishop *et al.* [2]. The flow is upward along the inner sphere and downward along the outer sphere. The center of the eddy, where ψ has its maximum value, is seen to lie in the upper half of the flow region at $\theta = 77°$, almost exactly half way between the two surfaces. The creeping-flow solution ${}^{(1)}\psi$, applicable in the limit of infinitesimal Rayleigh number, places the center of the eddy at $\theta = 90°$ and $(R - 1)/(R_o - 1) = 0{\cdot}49^+$; the effect of the finite Rayleigh number (1000) has been to move the center appreciably upward and very slightly outward. The upward and outward movement of the center of the eddy as the Rayleigh number is increased is in agreement with the experimental observations.

Let us define the "centerline" of the eddy to be the locus of points at which $\partial\psi/\partial R = 0$ in the open region $1 < R < R_o$, $0 < \theta < \pi$. So defined, this centerline passes through the center of the eddy and separates a subregion with positive V_θ from one with negative V_θ.

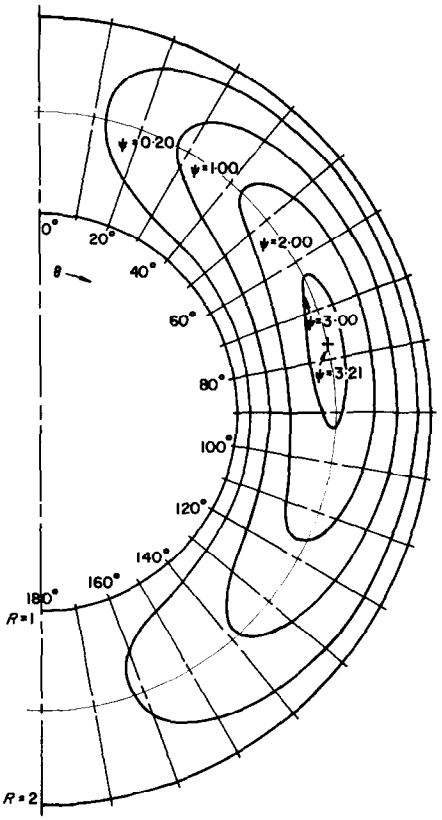

FIG. 1. Streamlines for $A = 1000$, $P = 0{\cdot}70$, $R_0 = 2{\cdot}00$.

Changing the Prandtl number from 0·70 to any other value in the range ($P > 0{\cdot}65$) for gases and non-metallic liquids has almost no effect on the streamline configuration (and hence on the nature of the velocity distribution). For flow in the liquid–metal range ($P < 0{\cdot}03$), however, the centerline of the eddy has an alignment which is rotated somewhat, relative to the alignment of the centerline for $P > 0{\cdot}65$, the sense of rotation being clockwise with respect to the viewpoint of Fig. 1.

For values of Rayleigh number greater than $A_{\text{lim}}/3$ yet sufficiently small that the series for ψ

still appears convergent, we find for $R_o = 1{\cdot}15$ and $P = 0{\cdot}70$ that a multicellular flow is predicted in which two secondary cells having a sense of rotation opposite to that of the primary central eddy are formed, one near $R = 1, \theta = 0°$ and the other near $R = R_o$, $\theta = 180°$. The presence of the secondary cells may be indicative of approaching a threshold of flow instability. With increasing Rayleigh number each secondary cell expands in size; it is probable that at some critical Rayleigh number the secondary cell at the top of the inner sphere becomes unstable and expands avulsively to trans-gap extent, thus triggering a subsequent unsteady motion. And indeed, the values of the gap Rayleigh number A^* for which the secondary cells are found for $R_o = 1{\cdot}15$ from our solution are comparable in magnitude to those for which unsteady (but apparently periodic) motion of the falling-vortices type was first observed experimentally for $R_o = 1{\cdot}19$ [2, 3].

3.3. *Velocity distributions*

The velocity components are related to the stream function by $V_R = (R^2 \sin\theta)^{-1}\, \partial\psi/\partial\theta$ and $V_\theta = -(R \sin\theta)^{-1}\, \partial\psi/\partial R$. In Fig. 2, we plot profiles of ${}^{(3)}V_R$ and ${}^{(3)}V_\theta$, obtained by differentiating ${}^{(3)}\psi$ in the above manner, for $A = 1000$, $P = 0{\cdot}70$ and $R_o = 2{\cdot}00$. The profile of ${}^{(3)}V_R$ is for $R = 1{\cdot}50$ (halfway between the spheres); it is seen that the speed of the radial outflow at $\theta = 0°$ is more than twice that of the radial inflow at $\theta = 180°$. Profiles of ${}^{(3)}V_\theta$ are shown in Fig. 2 for $\theta = n\,(40°)$, $1 \leqslant n \leqslant 4$; the most obvious (though not surprising) feature of these profiles is that the "upflow" speed near the inner sphere is much stronger than the downflow speed near the outer sphere. This feature is in agreement with the qualitative experimental observations of Bishop *et al.* [2].

3.4. *Temperature distribution*

For $A = 1000$, $P = 0{\cdot}70$, and $R_o = 2{\cdot}00$, Fig. 3 shows profiles of ${}^{(3)}T$ for $\theta = n(40°)$, $0 \leqslant n \leqslant 4$, as well as the temperature distribution ($T = T_0$) for pure conduction. At any particular radial position, $1 < R < R_o$, the temperature increases with decreasing θ. The smallness of the difference in temperature between the profiles for 120° and 160° implies that the local heat-transfer rates at both inner and outer spheres should be relatively independent of θ

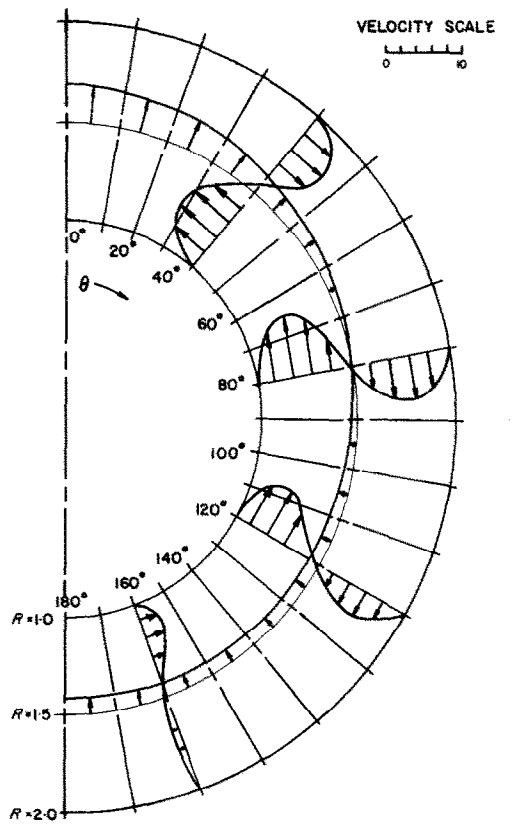

FIG. 2. Velocity profiles for $A = 1000$, $P = 0{\cdot}70$, $R_0 = 2{\cdot}00$.

for $120° \leqslant \theta \leqslant 180°$. The profile for $\theta°$ is predominantly concave downward, whereas that for 160° is predominantly concave upward.

Although the experimental temperature profiles of Bishop *et al.* [3] for $R_o = 2{\cdot}00$ were obtained for appreciably higher Rayleigh numbers so that direct comparison is not meaningful, we note that their profiles (see their Fig. 9) also exhibit the same ordering relative to one another, the closeness between profiles for 120° and 160°,

and the predominance of downward concavity in the profile for 0°.

3.5. *Heat-transfer rates*

We express q_i', q_o', and Q' by means of local and overall Nusselt numbers N_i, N_o, and $\bar{N}$ defined so as to be the ratios of the appropriate transfer rate at low Rayleigh numbers is a higher-order effect.

The local Nusselt numbers ${}^{(3)}N_i$ and ${}^{(3)}N_o$ are presented as functions of θ in Fig. 4 for $A = 1000$, $P = 0{\cdot}70$, and $R_o = 2{\cdot}00$. In comparison to its pure-conduction value the local heat-transfer rate has been increased for $65° < \theta \leqslant 180°$ of

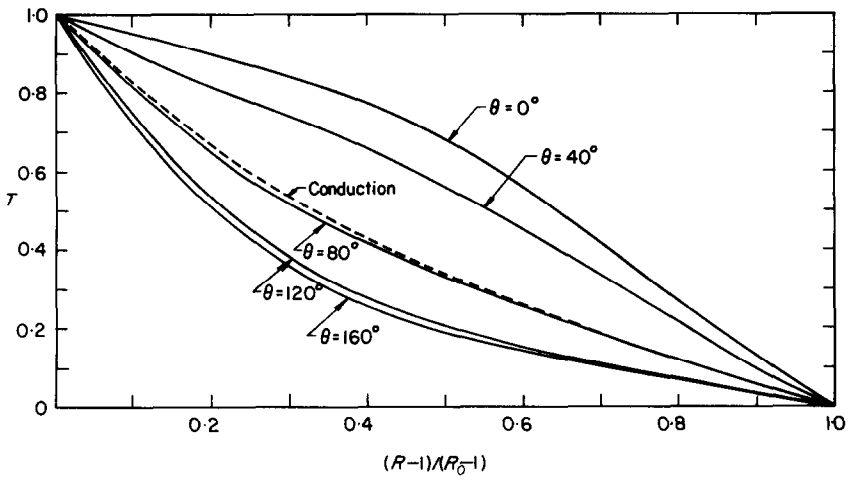

FIG. 3. Temperature vs. radial position for $\theta = n(40°)$, $0 \leqslant n \leqslant 4$, for $A = 1000$, $P = 0{\cdot}70$, $R_0 = 2{\cdot}00$.

local and overall effective thermal conductivities to the actual conductivity. Using Fourier's law of conduction, we have

$$N_{t,o} = -\frac{R_o - 1}{R_o}\left[R^2\frac{\partial T}{\partial R}\right]_{R=1,R_o}, \quad (28)$$

$$\bar{N} = -\frac{(R_o - 1)}{2R_o}\int_0^{\pi}\left[R^2\frac{\partial T}{\partial R}\right]_{R=1 \text{ or } R_o}\sin\theta\,d\theta. \quad (29)$$

Our best approximations for these Nusselt numbers are ${}^{(3)}N_i$, ${}^{(3)}N_o$, and ${}^{(3)}\bar{N}$, obtained by performing on ${}^{(3)}T$ the operations indicated. Although ${}^{(3)}N_i$ and ${}^{(3)}N_o$ depend on Prandtl number through the dependence of T_2 and T_3 on P, ${}^{(3)}\bar{N}$ is identically independent of Prandtl number. It may readily be shown that the first effect of P on $\bar{N}$ is of order A^4, so that the influence of Prandtl number on the overall heat-

the inner sphere and for $0° \leqslant \theta < 82°$ of the outer sphere, being reduced elsewhere. The deviation from the pure-conduction rate is greatest at $\theta = 0°$, the value of ${}^{(3)}N_o$ here being 2·66. The smallness of $|\partial^{(3)}N_{i,o}/\partial\theta|$ for $120° \leqslant \theta \leqslant 180°$ is in agreement with what was inferred in Section 3.4 from the temperature profiles for 120° and 160°. The fact that the value of θ for which the two local Nusselt numbers are equal is essentially the same as that at the center of the eddy (see Fig. 1) for this case is a coincidence. For the curves of Fig. 4, we find ${}^{(3)}\bar{N} = 1{\cdot}12$.

From their experimental measurements in the range $1{\cdot}4 \times 10^4 \leqslant A^* \leqslant 2{\cdot}5 \times 10^6$ and $1{\cdot}25 \leqslant R_o \leqslant 2{\cdot}5$ with air ($P = 0{\cdot}70$) Bishop *et al.* [3] developed a correlation for the overall heat transfer, given in our notation by

$$\bar{N} = 0{\cdot}106\,(A^*/0{\cdot}70)^{0{\cdot}276}. \quad (30)$$

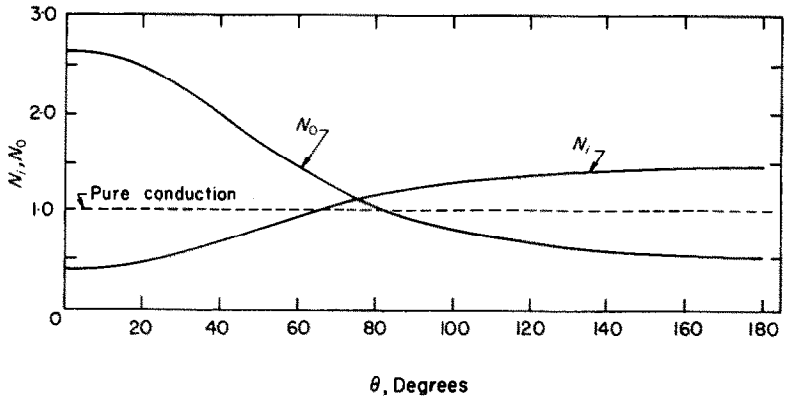

FIG. 4. Inner-sphere and outer-sphere local Nusselt numbers vs. angular position for $A = 1000$, $P = 0{\cdot}70$, $R_0 = 2{\cdot}00$.

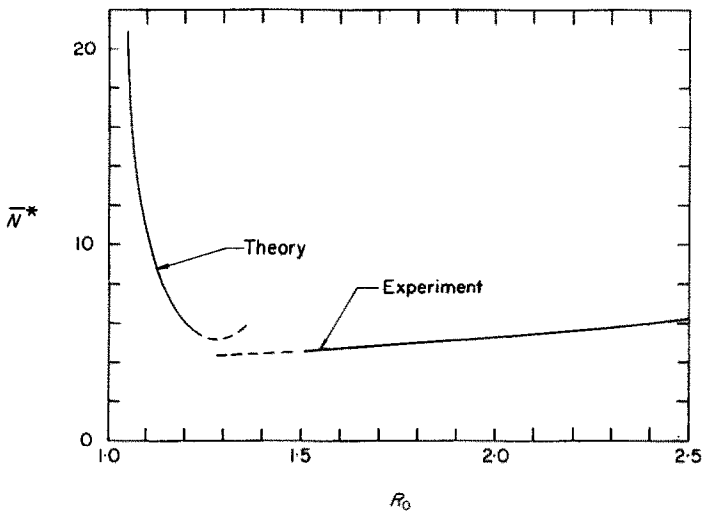

FIG. 5. $\bar{N}^*$ vs. R_0 to illustrate design for minimum heat loss for $A = 9 \times 10^4$, $P = 0{\cdot}70$. On dashed portion of theoretical curve, $A_{lim}/3 < 9 \times 10^4 < A_{lim}$. Dashed portion of experimental curve [see equation (30)] corresponds to values of A^* less than those of the data of Bishop *et al.* [3].

Although the range of applicability of the analytical solution and that of the experimental data show no overlap, we can utilize these results together in making a design application. Consider the design of a spherical insulating flask with specified radius of the inner shell to operate under a specified temperature difference between inner and outer shells. Heat transfer by conduction decreases while convection increases with increasing gap width. It is desired to find that radius of the outer shell for which the heat loss will be minimized. For specified fluid properties, then, both A and P are fixed, so that minimizing Q' with respect to R_o' is equivalent to minimizing $\bar{N}^*$ with respect to R_o. For $A = 9 \times 10^4$ and $P = 0{\cdot}70$, we plot both analytical and experimental determinations of $\bar{N}^*$ vs. R_o in Fig. 5. The dashed portion of the

experimental curve represents an extrapolation below the lowest value of A^* for which equation (30) was developed. On the other hand, the dashed portion of the theoretical curve indicates that for the corresponding values of R_o the Rayleigh number of 9×10^4 is between $A_{\text{lim}}/3$ and A_{lim}; for these values of R_o the predicted qualitative behavior should be reliable although the quantitative predictions may not be accurate. The analytical solution agrees reasonably well with the extrapolation of the experimental result; perhaps more importantly, it also correctly predicts the trend, for sufficiently large values of R_o, of increased heat transfer with increasing R_o, a trend observed experimentally for $R_o > 1{\cdot}5$. It is evident from Fig. 5 that the optimum radius ratio for the case considered is between 1·3 and 1·5. In connection with the thermal insulation of buildings, Batchelor [6] estimated in an analogous manner the optimum spacing of double windows and double walls to minimize heat loss in winter.

4. CONCLUSION

The solution of the governing equations for steady axisymmetric convection of fluid enclosed between isothermal concentric spheres has been obtained through the terms proportional to the third power of Rayleigh number in the series expansions of temperature and stream function. In general the streamline configuration is of the crescent-eddy type photographed by Bishop *et al.* [2]. For small radius ratios, however, and Rayleigh numbers approaching the limit for convergence of the series, local secondary eddies are noted which are interpreted to explain the inception of the unsteady falling-vortices flow observed experimentally [2, 3]. Velocity and temperature distributions are illustrated and discussed.

Local heat-transfer rates at both inner and outer spheres are expressed by means of local Nusselt numbers whose variation with angular position is portrayed. The overall heat-transfer rate is expressed by means of an overall Nusselt number, upon which the influence of Prandtl number is a higher-order effect entering only in terms of fourth and higher even powers of Rayleigh number. The analytical solution and the experimental data supplement each other; one manner in which they can be utilized together for design purposes is described.

ACKNOWLEDGEMENTS

The authors wish to thank Dr. L. G. Clark for several valuable suggestions. This paper is based in part on a Ph.D. dissertation (H.C.H.) submitted to the Graduate School of The University of Texas.

REFERENCES

1. E. H. Bishop, R. S. Kolflat, L. R. Mack and J. A. Scanlan, Photographic studies of convection patterns between concentric spheres, *Soc. Photo-opt. Instrum. Engrs Jl* **3**, 47–49 (1964–1965).
2. E. H. Bishop, R. S. Kolflat, L. R. Mack and J. A. Scanlan, Convective heat transfer between concentric spheres, in *Proceedings of the 1964 Heat Transfer and Fluid Mechanics Institute*, pp. 69–80. Stanford University Press, Stanford (1964).
3. E. H. Bishop, L. R. Mack and J. A. Scanlan, Heat transfer by natural convection between concentric spheres, *Int. J. Heat Mass Transfer* **9**, 649–662 (1966).
4. I. G. Sevruk, Transient heat convection within a spherical film, *J. Appl. Math. Mech.* **22**, 587–593 (1958).
5. H. C. Hardee, Jr., Natural convection between concentric spheres at low Rayleigh numbers, Ph.D. Dissertation, The University of Texas (1966).
6. G. K. Batchelor, Heat transfer by free convection across a closed cavity between vertical boundaries at different temperatures, *Q. Appl. Math.* **12**, 209–233 (1954).

Résumé—On a obtenue la solution pour la convection naturelle de révolution en régime permanent entre des sphères concentriques isothermes, en négligeant l'échauffement visqueux et en considérant comme constante chaque propriété du fluide sauf le poids spécifique. La configuration des lignes de courant, les distributions de vitesse et de température et les taux de transport de chaleur locaux et globaux sont discutés et illustrés. On a fait des comparaisons appropriées avec les résultats expérimentaux. La théorie et l'expérience se complètent l'une l'autre; un exemple modèle est donné dans lequel on a besoin des deux types de résultats.

Zusammenfassung—Unter Vernachlässigung der Reibungserwärmung und unter Annahme konstanter Stoffwerte mit Ausnahme der Dichte, wurde die Lösung für stationäre achssymmetrische freie Konvektion zwischen isothermen, konzentrischen Kugeln erhalten. Stromlinienanordnungen, Geschwindigkeits- und Temperaturverteilungen und sowohl der örtliche als auch der Gesamtwärmeübergang sind beschrieben und dargestellt. Entsprechende Vergleiche wurden mit Versuchsergebnissen durchgeführt. Theorie und Versuch ergänzen einander; in einem angegebenen Auslegungsbeispiel werden beide Ergebnisarten benötigt.

Аннотация—Получено решение для стационарной осесимметричной естественной конвекции между изотермическими концентрическими сферами при условии пренебрежения диссипативным нагревом и при условии постоянства всех свойств жидкости, за исключением удельного веса. В работе обсуждаются и иллюстрируются конфигурации линий тока, распределения скорости и температуры, а также локальные и суммарные тепловые потоки. Проведены соответствующие сравнения с экспериментальными результатами. Теория и эксперимент дополняют друг друга. Приводится расчет, для которого необходимы как теоретические, так и экспериментальные результаты.